JOURNAL OF NANO- AND ELECTRONIC PHYSICS
Vol. **7** No 3, 03044(5pp) (2015)

ЖУРНАЛ НАНО- ТА ЕЛЕКТРОННОЇ ФІЗИКИ
Том **7** № 3, 03044(5cc) (2015)

Influence of Ion Implantation on the Structural and Stressed State and Mechanical Properties of Nitrides of High-entropy (TiZrAlYNb)N and (TiZrHfVNbTa)N Alloys

O.V. Sobol'[1], I.V. Yakushchenko[2,*]

[1] *National Technical University "Kharkiv Polytechnic Institute", 21, Frunze Str., 61002 Kharkiv, Ukraine*
[2] *Sumy State University, 2, Rimsky-Korsakov Str., 40007 Sumy, Ukraine*

(Received 16 August 2015; revised manuscript received 17 October 2015; published online 20 October 2015)

As a result of deposition of nanostructured multicomponent (TiZrAlYNb)N and (TiZrHfVNbTa)N nitride coatings, a phase with FCC lattice and crystallite sizes from 7 nm to 17-20 nm, respectively, is formed. Compressive stresses are developed, with values of – 2.97 GPa and – 3.86 GPa for 6-elements nitrides, and – 0.25 GPa and – 3.14 GPa for 5-elements coatings. Dependence of the stress change on the nitride concentration in the coatings is found, and possible reasons of the observed correlation are discussed. Ion implantation of Au-leads to disorder of the coatings structure in the implanted layer, decrease in nanocrystallite sizes, and, as a result, increase in nanohardness of the coatings to 39 GPa.

Keywords: Nitrides of high-entropy alloys, Vacuum-arc cathode evaporation, Phase and elemental composition, Hardness, Ion implantation, Negative ions.

PACS number: 81.40.Wx

1. INTRODUCTION

A search for new coatings with increased functional properties based on transition metals led to the creation of a novel class of multi-element alloys, the so-called high-entropy alloys (HEA) [1-10]. In HEA, formation of the structures with characteristics resistant to high temperatures occurs based on the thermodynamic principles at content not less than 5 primary elements with atomic concentration from 5 % to 35 % [11-13]. The distinctive feature of HEA is that mixing of 5 and more elements leads to the formation of a stable substitutional solid solution with relatively simple cubic (fcc and bcc) or hexagonal crystal lattices, but not intermetallics or multiphase structure as in the case of traditional multi-element alloys.

The obtained materials are sufficiently high-strength and thermodynamically stable that predetermines their increased resistance to chemical corrosion and wear, improves the mechanical properties, etc. [11-14].

Nitrides and carbides based on HEA demonstrate higher physical and mechanical properties that has aroused great interest of researchers and practitioners to this type of coatings. Moreover, the study of the influence of such a traditional coating treatment method as ion implantation on the structural-phase changes and mechanical characteristics of the coatings is an actual problem. To this end, negative Au^- ions, which were implanted to the dose of 1×10^{17} cm^{-2} at accelerating voltage of 60 kV, were selected. The choice of Au ions is grounded by two factors: the processes based on them can be strongly identified (for example, using the Rutherford ion backscattering method), and also with the fact that the majority of elements of the studied high-entropy coating (Ti, Zr, Hf, Nb, Ta) do not interact with gold with the formation of intermetallics or other phases.

2. EXPERIMENTAL

5-element Ti-Zr-Al-Y-Nb and 6-element Ti-Zr-Hf-V-Nb-Ta cathodes of HEA were obtained by the vacuum-arc melting of metallic cathodes in a water-cooled copper vessel. To form the necessary homogeneity of the cathodes, they were repeatedly (5-7 times) re-melted [24]. Production of the coatings was performed by the vacuum-arc plant "Bulat-6". Pulsed deposition mode was used to increase the plasma flow energy, improve the adhesion properties of the obtained coatings and manufacture more dispersive coating structure. Steel disks and plates (steel 12X18H9T) of 45 mm diameter and 4 mm thickness were used as the substrate.

Scanning electron microscope with energy-dispersion spectrometer JSM-6010 LA (JEOL, Japan) was used to study the surface of multicomponent coatings, their elemental composition and distribution of elements over the coating surface. Measurements of the microhardness were performed on the device REVETEST (Switzerland), and nanohardness and elastic modulus were studied in the dynamic mode on Triboindentor TI-950 (HYSITRON Inc.).

Measurements of the phase composition of the coatings were carried out by two X-ray diffractometers DRON-3M in Cu-Kα radiation and RINT-2500 V using position-sensitive proportional counter (PSPC/MDGT) in Cr-Kα radiation. The measurements were conducted at angles of 3°, 10°, and 30° for the samples in the initial state (after coating deposition) and at an angle of 2° for the samples which underwent implantation by Au^- ions.

A nonstandard (compared with the most frequently used in the case of cubic lattices $a - \sin^2\psi$ method [15]) technique was utilized to determine the stressed state of the coatings. It is based on plotting of the graph at fixed initial angles of the sample (θ) when taking the whole spectrum ($\theta = 3°$, 10° or 30°). The calculations were carried out for the diffraction peaks corresponding to the reflections from the plane (220) in the angular range of the counter of $2\theta = 110°\ldots120°$.

---

[*] kosistivan@gmail.com

Measurements of the hardness and reduced modulus of elasticity of the coatings were performed by the nanoindentation method on the equipment Hysitron TriboIndenter 950 using Berkovich diamond pyramid (Ti-0039, vertex angle 142.3°, nose radius 100 nm) calibrated by quartz. The maximum load during measurements was chosen to prevent the influence of the substrate on the measured values. To measure the hardness and reduced modulus of elasticity at different depths of the coating, the load of the form of a trapezoidal sine with step-by-step increasing load from 0.05 μN to 10 μN was applied to the indenter, at that load duration 3 s, exposure 0.5 s, unloading 3 s.

3. RESULTS AND DISCUSSION

Deposition parameters and elemental composition of the coatings (obtained using energy-dispersion analysis) are given in Table 1 for both types of coatings. In Fig. 1 we illustrate the energy-dispersion spectrum for the five-element coating.

Results of the elemental analysis of the coatings indicate that active resputtering processes occur at higher vacuum in the working chamber during the coating production, and, as a result, the coating is depleted with nitrogen, while the relative concentration of metal atoms increases. According to [16-21], this should influence the structural-phase composition of the coatings and their stressed state, the investigation results of which for alloys before and after implantation will be given below.

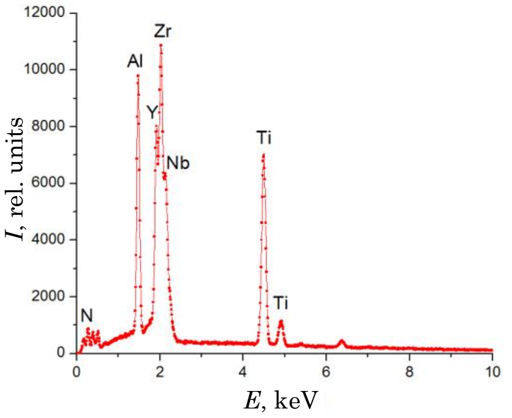

Fig. 1 – Energy-dispersive spectrum of the sample of series 1

In Table 2 we present the values of the lattice parameters for binary nitrides of the metal components. As seen, there is a significant difference in both the stability of the formed nitrides (enthalpy and entropy of their formation [22]) and the lattice parameters defined by the atomic radiuses of the metal component. The difference of the last ones has determined high values of the stress-strain state of nitride HEA as it was shown in [23, 24].

To perform the phase-structural studies, Cu-Kα and Cr-Kα radiations were used (at that, the latter in both the standard and the sliding geometries) that allowed to compare the bulk state with the surface modified state of the coating after ion irradiation.

In Fig. 2a, b we show the X-ray diffraction spectra of the coatings of (TiZrAlYNb)N and (TiZrHfVNbTa)N systems, respectively.

Spectrum analysis of the 5-element coatings implies that the fcc-phase content increases in the surface layers with increasing pressure and saturation of the coating with nitrogen. We should also note the change in the preferred growth orientation of the fcc-crystallites with increasing pressure: from (111) at low pressure to (200) at high pressure (spectra 1 and 3 in Fig. 2a).

The crystallite size also varies. Thus, for the coatings of the second series, crystallite size of the bcc-phase is sufficiently small and is about 7.7 nm. An increase in the nitrogen pressure leads to the increase in the bcc-crystallite sizes of the sample of the first series up to 11.5 nm and fcc-phase up to 5 nm. Crystallites of the samples of the third series have average sizes of 10 nm for the bcc-phase and about 7 nm – for the fcc-phase.

For 6-element coatings, the results are the following. The phase with the fcc-lattice and preferred orientation of the crystallites growth with the axis [100] is formed in the manufacture of the coatings using the working gas pressure of 3×10^{-4} torr. The average crystallite size of the fcc-phase is equal to 8 nm. At elevated pressure of 3×10^{-3} torr, the structural state is changed as a result of the formation of a new texture type with axis [111] that is manifested in the form of a substantial increase in the relative intensity of the peaks from the corresponding plane. Moreover, crystallite size of the fcc-phase of the coating also increases, which is about 17-20 nm.

Calculation results of the stressed state as well as the values of the macrostrain of the crystal lattice are represented in Table 3.

Table 1 – Deposition parameters and elemental composition of the coatings

Series number	Material	U_b, V	P, torr	Concentration, wt. %						
				N	Ti	Zr	Al	Y	Nb	
1	(TiZrAlYNb)N	– 150	1.2×10^{-3}	46.00	15.55	11.47	10.29	10.74	5.96	
2			4×10^{-4}	35.25	18.92	12.86	15.20	10.94	6.84	
3			4×10^{-3}	57.76	12.45	8.75	6.81	8.81	5.42	
				N	Ti	Zr	Hf	V	Nb	Ta
4	(TiZrHfVNbTa)N	– 150	3×10^{-3}	54.38	6.97	8.46	11.22	4.96	9.86	4.15
5			3×10^{-4}	45.70	9.05	9.85	12.91	5.65	12.18	4.67

Table 2 – Lattice parameters, entropy, and enthalpy of the binary nitride formation

	TiN	ZrN	AlN	YN	NbN	TaN	HfN
Lattice parameters (a), nm	0.4242	0.4578	0.436	0.4877	0.4394	0.4307	0.4524
Entropy of formation, J/mole·deg.	30.31	38.93	20.93	46.05	43.96	42.7	40.0
Enthalpy of formation, kJ/mole	336.62	365.51	320.29	299.36	237.81	252.7	374.0

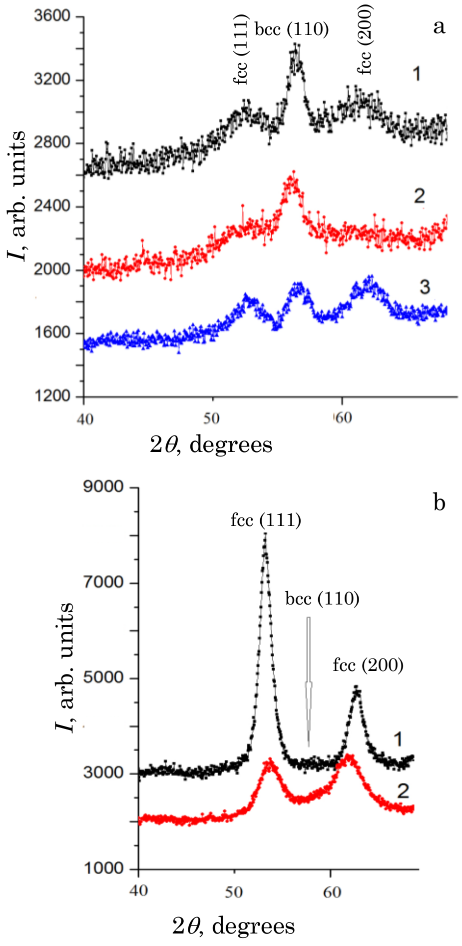

Fig. 2 – Regions of the diffraction spectra obtained in the sliding geometry (3°, Cr-Kα-radiation) of the coatings of the systems: a) (TiZrNbYAl)N deposited at different P_N (torr): 1 – $1.2\cdot10^{-3}$, 2 – $4\cdot10^{-4}$, 3 – $4\cdot10^{-3}$; b) (TiZrHfVNbTa)N obtained at different P_N (torr): 1 – $3\cdot10^{-3}$, 2 – $3\cdot10^{-4}$

Table 3 – The determination results of the macrostrain and stress in the studied coatings

Series No	ε, %	σ, GPa
4	– 1.80	– 3.86
	– 1.31	
	– 0.58	
5	– 1.11	– 2.97
	– 1.38	
	– 0.35	
1	– 1.88	– 3.14
	– 0.46	
2	– 0.15	– 0.25
	– 0.07	

In Fig. 3 we illustrate the dependences of the lattice parameter of the coatings (TiZrAlYNb)N (samples of the series 1, 2) and (TiZrHfVNbTa)N (samples of the series 4, 5) on $\sin^2\psi$.

As seen, the compressive stresses are developed in the coatings that is typical for vacuum-arc coatings obtained when using a negative bias voltage ($U_b = -150$ V in this case). Stresses decrease from – 3.86 GPa (sample of the series 4) to – 2.97 GPa (sample of the series 5) with changing working gas pressure for 6-element nitrides from $3\cdot10^{-3}$ torr to $3\cdot10^{-4}$ torr.

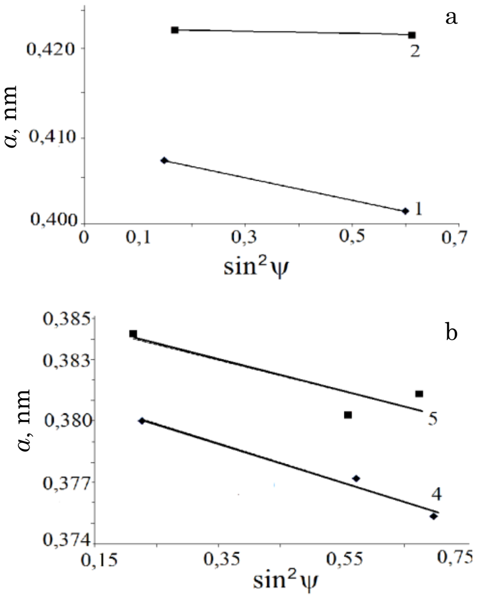

Fig. 3 – Dependences $a - \sin^2\psi$ obtained by the crystalline group method for the texture axis [110] of the coating of HEA of the (TiZrAlYNb)N (a) and (TiZrHfVNbTa)N (b) systems

The situation is quite different in the case of the 5-element nitrides. In the coating of the sample of the series 2 one can observe a very low strain, and compressive stress is equal to – 0.25 GPa. For the sample of the series 1, compressive stress makes – 3.14 GPa.

As known, the presence of voids in the octahedral positions of nitrogen atoms in the lattice can make a great contribution to the compressive strain. In Fig. 4 we show the dependence of σ on the nitrogen concentration N.

As seen from Fig. 4, there is a tendency to increase compressive stresses with increasing nitrogen concentration in the coating. One can suggest that the increase in the working gas pressure leads to the fact that larger number of nitrogen atoms is embedded in the octahedral voids of the crystal lattice (since it is known that constituent atoms in HEA have equal probability to occupy one or another position in the lattice). This, in turn, causes the development of compressive stresses in the coating.

In Fig. 5 we illustrate the dependences of the nanohardness and reduced modulus of elasticity on the penetration depth of the Berkovich pyramid [25, 26] into the coating of the series 4 in dynamic indentation. In the im-

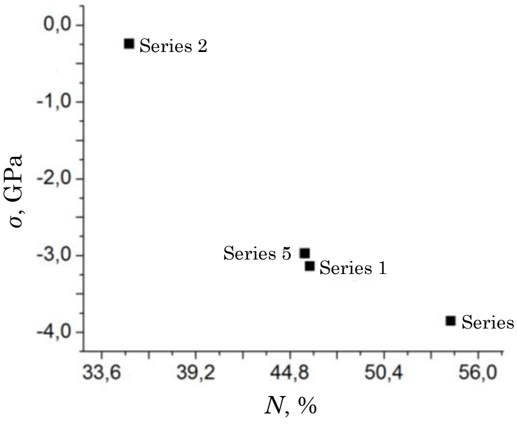

Fig. 4 – Dependence of the stress σ on the Ni concentration N

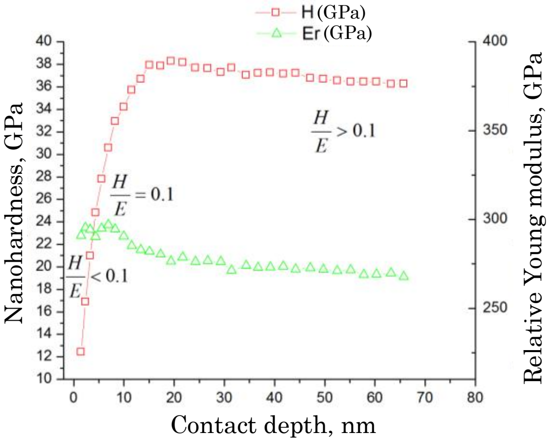

Fig. 5 – Dependences of the nanohardness and reduced modulus of elasticity on the indenter penetration depth into the coating obtained at $U_b = -150$ V, $P = 3.0 \times 10^{-3}$ torr

planted layer, at a depth of (15÷25) nm one can observe an increase in the nanohardness up to almost 39 GPa with a gradual attainment of the horizontal line at the penetration depth of 70 nm; and increase in the plasticity index in the implanted region – $H / E \geq 0.1$ indicates the increase in the wear resistance. Thus, implantation of heavy Au^- ions leads to excess of hardness and excess of plasticity index.

We should note that Au^- ions have high sputtering yield [27]. Therefore, in high-dose implantation, a partial sputtering from the surface of N atoms occurs due to their weaker coupling. Formation of a high density of individual cascades of the shifted atoms (substitutional solid solution) occurs during implantation; and defects [28], namely, vacancy and interstitial loops are formed with high efficiency. Implanted Au^- ions form the ball-shaped nanocrystallites in the coating of size of several nm (as it was shown during Cu^-, Au^- ion implantation into SiO_2 in [29-31]). In the nanostructured coating, efficiency of recombination of point defects increases near cascades (or inside them) due to proximity of the interfaces [28]. Moreover, during implantation with heavy ions, percentage of interfaces increases because of grinding (fragmentation) of nanograins from 8 to 5 nm and less (as it was shown in the study of the structural and phase state), thanks to which formation of the disordered polycrystalline structure without preferred orientation of the fcc-phase takes place. Also, the formed defects, grain boundaries, etc. are an obstacle to the extension of dislocations in plastic deformation of the material. And since hardness of the substance characterizes its resistance to elastic and plastic deformations during indentation of a counterbody, one can assume that the obtained nanostructural coatings have a noticeably higher resistance to radiation with Au^- ions compared with single crystals and polycrystals [18], and ion implantation leads to the improvement of the mechanical properties of the coatings.

4. CONCLUSIONS

1. In the case of the 5-element coatings of the system (TiZrNbYAl)N, the evolution of the structural state from amorphous to nanocluster, and then to nanocrystalline one occurs with increasing working gas pressure. Formation of two crystalline phases with the fcc- and bcc-lattices, whose ratios in the coating vary with changing deposition parameters, takes place.

2. In the 6-element (TiZrHfVNbTa)N nitrides, amorphous phase formation at a lower working gas pressure is not observed. Texture axis [111] is the preferred direction of crystallite growth. The phase with the fcc-lattices is formed as the main crystalline phase; the bcc-phase is observed for the coatings obtained at the highest pressure of $3 \cdot 10^{-4}$ torr in the near-surface layer.

3. The studied 5- and 6-element coatings of the nitrides (TiZrNbYAl)N and (TiZrHfVNbTa)N demonstrate higher resistance to radiation under ion implantation of Au^- than traditional nitrides of the transition metals.

ACKNOWLEDGEMENTS

The authors of the paper express their gratitude to Prof. A.D. Pogrebnjak for valuable discussions and useful comments on the work; Dr. Tech. Sci. A.A. Andreev for the provided coating samples, and Prof. K. Oyoshi and Prof. Y. Takeda for the unique irradiation with negative Au^- ions.

REFERENCES

1. J.-W. Yeh, Y.-L. Chen, S.-J. Lin, *Mater. Sci. Forum* **560**, 1 (2007).
2. N. Wanderka, S. Singh, U. Glatzel, J. Banhart, *Acta Materialia* **59**, 182 (2011).
3. S. Ranganathan, *Curr. Sci.* **85** No 10, 1404 (2003).
4. A. Inoue, *J. Appl. Phys.* **87**, 1141 (2000).
5. V. Dolique, A-L. Thomann, P. Brault, Y. Tessier, P. Gillon, *Mater. Chem. Phys.* **117**, 142 (2009).
6. V. Dolique, A.-L. Thomann, P. Brault, Y. Tessier, P. Gillon, *Surf. Coat. Technol.* **204**, 1989 (2010).
7. M.-H. Tsai, C.-W. Wang, C.-W. Tsai, W.-J. Shen, J.-W. Yeh, J.-Y. Gan, W.-W.Wu, *J. Electrochem. Soc.* **158** No 11, H1161 (2011).
8. A. Li, X. Zhang, *Acta Metall. Sin. (Engl. Lett.)* **22** No 3, 219 (2009).
9. C.H. Lai, S.J. Lin, J.W. Yeh, S.Y. Chang, *Surf. Coat. Technol.* **201**, 3275 (2006).
10. M. Braic, V. Braic, M. Balaceanu, C.N. Zoita, A. Vladescu, E. Grigore, *Surf. Coat. Technol.* **204**, 2010 (2010).
11. Y. Zhang, T.T. Zuo, Z. Tang, M.C. Gao, K.A. Dahmen, P.K. Liaw, Z.P. Lu, *Prog. Mater. Sci.* **61**, 1 (2014).
12. B.S. Murty, Jien-Wei Yeh, S. Ranganathan, *High-Entropy Alloys* (Oxford: Butterworth-Heinemann: 2014).
13. A.D. Pogrebnjak, A.A. Bagdasaryan, I.V. Yakuschenko, V.M. Beresnev, *Russ. Chem. Rev.* **83**, 1027 (2014).
14. O.V. Sobol', A.A. Andreev, V.A. Stolbovoi, V.E. Fil'chikov, *Tech. Phys. Lett.* **38** No 2, 168 (2012).
15. C. Genzel, W. Reinmers, *phys. status solidi (a)* **166** No 2, 751 (1998).
16. X. Feng, G. Tang, X. Ma, M. Sun, L. Wang, *Nucl. Instr. Meth. Phys. Res. B* **301**, 29 (2013).
17. A.D. Pogrebnjak, I.V. Yakushchenko, A.A. Bagdasaryan, O.V. Bondar, R. Krause-Rehberg, G. Abadias, P. Chartier, K. Oyoshi, Y. Takeda, V.M. Beresnev, O.V. Sobol, *Mater. Chem. Phys.* **147** No 3, 1079 (2014).
18. A.D. Pogrebnjak, *J. Nanomater.* **2013**, ID 780125 (2013).
19. A.D. Pogrebnjak, V.M. Beresnev, *Nanocoatings Nanosystems Nanotechnologies* (Oak Park, IL: Bentham Science Publishers: 2012).
20. P. Misaelides, A. Hatridimitriou, F. Noli, A.D. Pogrebnjak,

Y.N. Tyurin, S. Kosionidis, *Surf. Coat. Technol.* **180-181**, 290 (2004).
21. A.D. Pogrebnjak, A.G. Lebed, Yu.F. Ivanov, *Vacuum* **63**, 483 (2001).
22. H.V. Samsonov, *Nitridy* (Kyev: Naukova dumka: 1969).
23. R. Krause-Rehberg, A.D. Pogrebnyak, V.N. Borisyuk. M.V. Kaverin, A.G. Ponomarev, M.A. Bilokur, K. Oyoshi, Y. Takeda, V,M. Beresnev, O.V. Sobol', *Phys. Metal. Metallography* **114** No 8, 672 (2013).
24. O.V. Sobol', A.A. Andreev, V.F. Gorban', N.A. Krapivka, V.A. Stolbovoi, I.V. Serdyuk, V.E. Fil'chikov, *Tech. Phys. Lett.* **38** No 7, 616 (2012).
25. A.D. Pogrebnjak, I.V. Yakushchenko, O.V. Sobol, V.M. Beresnev, A.I. Kupchishin, O.V. Bondar, M.A. Lisovenko, H. Amekura, K. Kono, K. Oyoshi, Y. Takeda, *Techn. Phys.* **60** No 8, 1176 (2015).
26. A.D. Pogrebnyak, I.V. Yakushchenko, O.V. Bondar, O.V. Sobol, V.M. Beresnev, K. Oyoshi, H. Amekura, Y. Takeda, *Phys. Solid State* **57** No8, 1556 (2015).
27. B. Schmidt K. Wetzig, *Ion Beams in Materials Processing and Analysis.* (Wien: Springer-Verlag: 2013).
28. N.A. Azarenkov, O.V. Sobol', A.D. Pogrebnyak, V.M. Beresnev, S.V. Litovchenko, O.N. Ivanov, *Materialovedeniye neravnovesnogo sostoyaniya modifitsirovannoy poverkhnosti: monografiya* (Sumy: Sumskiy gosudarstvennyy universitet: 2012) [in Russian].
29. D. Debi, Y. Takeda, H. Amekura, M. Sasase, N. Kishimoto, *Appl. Surf. Sci.* **310**, 164 (2014).
30. V.I. Lavrentiev, A.D. Pogrebnjak, *Surf. Coat. Tech.* **99**, 24 (1998).
31. A.D. Pogrebnjak, A.P. Kobzev, B.P. Gritsenko, S. Sokolov, E. Bazyl, N.V. Sviridenko, A.N. Valyaev, Y.F. Ivanov, *J. Appl. Phys.* **87**, 2142 (2000).